*Journal of the European Ceramic Society* **10** (1992) 101–107

# Weakest-link Failure Predictions for Ceramics III: Uniaxial and Biaxial Bend Tests on Alumina

B. J. de Smet, P. W. Bach

Netherlands Energy Research Foundation (ECN), P.O. Box 1, 1755 ZG Petten, The Netherlands

&

H. F. Scholten, L. J. M. G. Dortmans, G. de With*

Centre for Technical Ceramics, P.O. Box 595, 5600 AN Eindhoven, The Netherlands

(Received 22 July 1991; revised version received 4 November 1991; accepted 7 November 1991)

***Abstract***

*To obtain a complete and reliable data set of Weibull parameters for the validation of numerical models for weakest-link failure probability calculations on ceramic components, uniaxial (three- and four-point) and biaxial (ball-on-ring and ring-on-ring) bend tests were performed on two aluminas. With the uniaxial data sets, the biaxial experiments were predicted applying two fracture criteria, the mode I failure and the maximum noncoplanar strain energy release rate for penny-shaped cracks. The best fitting criterion for the materials turns out to be different showing a marked difference in their shear stress sensitivity.*

*Um die Gültigkeit numerischer Modelle für die Berechnung der Versagenswahrscheinlichkeit schwächster Bindungsstellen in keramischen Bauteilen zu überprüfen, wurden zur Erstellung eines vollständigen und verläßlichen Datensatzes von Weibull-Parametern uniaxiale (d.h. Drei-Punkt- und Vier-Punkt-Biegeversuche) und biaxiale (d.h. Kugel-auf-Ring- und Ring-auf-Ring-Biegeversuche) Biegeversuche mit zwei verschiedenen Aluminiumoxid-Keramiken durchgeführt. Mit Hilfe des Datensatzes über die uniaxiale Beanspruchung konnten die biaxialen Experimente vorhergesagt werden, und zwar indem zwei Bruchkriterien hierbei herangezogen wurden: einerseits Versagen unter Mode I und andererseits maximale Freisetzungsrate der nicht coplanaren Verformungsenergie für den Fall mondförmiger Risse. Es zeigt sich, daß das Kriterium, welches jeweils das Verhalten der untersuchten Werkstoffe am besten beschreibt, deutlich von der Empfindlichkeit des Materials gegenüber Scherspannungen abhängt.*

*Pour vérifier la validité des modèles numériques en ce qui concerne les calculs de probabilité de rupture du maillon le plus faible dans des composants céramiques, des essais uniaxiales de flexion (trois et quatre points) et biaxiales (bille sur anneau et anneau sur anneau) ont été réalisés sur deux alumines différentes pour obtenir une liste complète et fiable de paramètres Weibull. A l'aide des données uniaxiales, les expériences biaxiales ont été prédites en applicant, deux critères de fracture, le mode I de rupture et le taux maximum de libération d'énergie de déformation sous charge noncoplanaire pour des fissures prismatiques. Le critère le plus adapté pour les deux matériaux semble différent car ils montrent une différence marquée dans leur sensibilité à la contrainte de cisaillement.*

## 1 Introduction

Validation of models for failure probability calculations of ceramic components requires multiaxial test data to select the fracture criterion that can best be applied.[1] For this selection, e.g. the failure probability of biaxial tests (ball-on-ring and ring-on-ring tests) can be predicted with the results of uniaxial tests (three-point and four-point bend tests) and compared with experimental data. This prediction requires high experimental reliability.

Tests with an accuracy better than 1·5% can be

* Also affiliated with Philips Research Laboratories, P.O. Box 80000, 5600 JA Eindhoven, The Netherlands.



*Journal of the European Ceramic Society* 0955-2219/92/$5.00 

done at the Centre for Technical Ceramics (CTK) and the Netherlands Energy Research Foundation (ECN), as shown in the previous paper.[2] In the present paper tests on a commercially available alumina and a laboratory-scale alumina are reported. The uniaxial tests were performed at the ECN and the biaxial tests at the CTK. The data to be used in the failure probability calculations were determined from the results of three-point bend tests, four-point bend tests, ball-on-ring tests and ring-on-ring tests. Two fracture criteria, the mode I (or normal stress) failure and the maximum non-coplanar energy release rate criterion are then applied to predict the mean fracture strength of the biaxial tests. Comparison of these predictions with the experimental data allows the judging of the validity of a particular failure model.

## 2 Experimental Procedure

### 2.1 Materials

A commercially available alumina (AL-997, Wesgo, USA) and a laboratory-scale alumina (National Ceramic Centre, NKA/ECN) were chosen to obtain the data series. The Wesgo sample contains 99·7% alumina. The laboratory alumina was fabricated from Alcoa A16SG powder (99·7% $Al_2O_3$) by cold isostatic pressing at 200 MPa. Bars of $50 \times 50 \times 200$ mm and rods of $\phi 50 \times 200$ mm were presintered at 1100°C for 30 min and subsequently sectioned into 5-mm thick plates and 2-mm thick disks and sintered in air at 1550°C for 4 h.

The microstructures of the two materials were revealed by thermal etching. The Wesgo alumina was etched for 3 h at 1400°C and the NKA alumina was etched for 20 min at 1500°C. Subsequently, photographs were made from which the grain contours were digitized and numerically processed. The statistical analysis represented in Table 1 gives the results of a least-squares fit on the area of the scanned grains (491 for the Wesgo alumina and 218 for the NKA alumina). The grains of the Wesgo alumina are fairly homogeneously distributed. However, the microstructure of the NKA alumina is bimodal. The grains of this material can be subdivided into two fractions of 50% and 42% respectively.

Analysis of the micrographs in two mutual perpendicular directions showed that neither of the materials contained a preferred orientation. For the preparation of the Wesgo alumina disks, as-sintered bricks were used ($300 \times 100 \times 50$ mm). The bricks were cut into sheets with a D91 grid wheel, from which the disks were ground with a D61 grid wheel. The ball-on-ring disks (10 mm in radius and 1·5 mm in thickness) were ground in three steps with a D46, D25 and a D15 grid wheel until finally a roughness ($R_a$) of about 0·3 $\mu$m was obtained. The ring-on-ring disks (15 mm in radius and 1·5 mm in thickness) and the bend bars were prepared analogously. For the ring-on-ring disks this resulted in a roughness of about 1 $\mu$m. No further edge finish was applied.

**Table 1.** Microstructural characterization of the tested aluminas

| | *Wesgo alumina* | *NKA alumina* | |
|---|---|---|---|
| Grains counted | 491 | 218 | |
| Mean perimeter, $\mu$m | 121·9 | 72·9 | |
| Mean grain area, $\mu m^2$ | 1 233 | 729 | |
| Least-squares fit of the area distribution to a log-normal distribution | | | |
| Fraction, % | 98 | 50 | 42 |
| $D$ (50%) | 520 | 177 | 168 |
| $s$ | 3·58 | 4·33 | 2·02 |

$D$ (50%) denotes the median value for the area distribution while $s$ denotes the geometric standard deviation of the log-normal distribution.

The NKA alumina bars were prepared from as-sintered sheets ($5 \times 45 \times 60$ mm). The sheets were ground to a thickness of $4{\cdot}5 \pm 0{\cdot}05$ mm with a $\phi 250 \times 10$ mm diamond grid wheel type 1A1-D126-C75-resin bonded (rotational speed 30 m/s and feeds 10 $\mu$m per pass and 15 mm/min). After that the sheets were cut to bars with a width of 3·7 mm and a length of 50 mm, using a $\phi 150 \times 0{\cdot}6$ mm diamond grid wheel type 1A1R-D181-C75-resin bonded (rotational speed 32 m/s and feed 15 mm/min). Afterwards the bars were ground with the D126 grid wheel to a width of $3{\cdot}5 \pm 0{\cdot}05$ mm and the corners were 0·1 mm chamfered (45°).

The NKA alumina disks were prepared from as-sintered disks. The final dimensions (15 mm in radius and 1·5 mm in thickness) were obtained by grinding with the D126 grid wheel. The applied rotational speed and feed were equal to that applied for preparing the bars. The roughness, $R_a$, of both bars and disks was 0·3 $\mu$m.

Utmost care was taken to reach the same surface condition for all types of specimens. The properties of the materials and the dimensions of the specimens are listed in Table 2. Young's modulus $E$ and Poisson's ratio $\nu$ were determined by the pulse-echo technique. The fracture toughness was determined from the maximum load of four-point bend tests on chevron-notched bars.

**Table 2.** Material properties and specimen dimensions

| *Wesgo alumina* | | *NKA alumina* | |
|---|---|---|---|
| Young's modulus ($E$) = 369 GPa<br>Poisson's ratio ($\nu$) = 0·237<br>density ($\rho$) = 3·85 kg/dm$^3$<br>mean grain size ($d$) = 50 $\mu$m<br>fract. toughness ($K_{Ic}$) = 3·85 MPa$\sqrt{m}$ | | Young's modulus ($E$) = 377 GPa<br>Poisson's ratio ($\nu$) = 0·24<br>density ($\rho$) = 3·89 kg/dm$^3$<br>mean grain size ($d$) = 10 $\mu$m<br>fract. toughness ($K_{Ic}$) = 4·5 MPa$\sqrt{m}$ | |
| *Bars* | *Disks* | *Bars* | *Disks* |
| $l$ = 50 mm | $R$ = 10 mm (BOR) | $l$ = 50 mm | |
| $w$ = 3·5 mm | $R$ = 15 mm (ROR) | $w$ = 3·5 mm | $R$ = 15 mm (ROR) |
| $h$ = 4·5 mm | $t$ = 1·5 mm | $h$ = 4·5 mm | $t$ = 1·5 mm |
| $c$ = 0·17 mm | $f \leq 5$ $\mu$m | $c$ = 0·1 mm | $f \leq 5$ $\mu$m |
| $f \leq 5$ $\mu$m | Pp $\leq 5$ $\mu$m | $f \leq 5$ $\mu$m | Pp $\leq 5$ $\mu$m |
| Pp $\leq 5$ $\mu$m | $R_a$ = 0·3 $\mu$m (BOR) | Pp $\leq 5$ $\mu$m | $R_a$ = 0·3 $\mu$m |
| $R_a$ = 0·3 $\mu$m | $R_a$ = 1·0 $\mu$m (ROR) | $R_a$ = 0·3 $\mu$m | |

ROR = Ring-on-ring; BOR = ball-on-ring; $l$ = length; $w$ = width; $h$ = height; $c$ = chamber; $R$ = radius; $t$ = thickness; $f$ = flatness; Pp = planparallellism; $R_a$ = roughness.

## 2.2 Test set-up

In Ref. 2 the uniaxial and biaxial bend fixtures were described and analysed in detail. With the fixtures bend tests can be performed within an accuracy of $< 1{\cdot}5\%$. In order to maintain equal conditions for each strength test and to minimize influences of subcritical crack growth, all tests were performed at a strain rate of $5 \times 10^{-4}$ per second in a nitrogen environment with a dew point of $-35°C$ (relative air humidity of 0·8%). For the latter purpose, perspex chambers were added to the experimental set-ups from Ref. 2. The prescribed humidity was established by means of a constant nitrogen gas flow and measured with a hydrometer (Panametrics system 3A).

Series of 40 Wesgo alumina and 20 NKA alumina specimens were tested under the conditions listed in Table 3. One Wesgo alumina series was tested in four-point bending, two in three-point bending (short and long span), one in ball-on-ring bending and one in ring-on-ring bending. Erroneously, one batch of Wesgo alumina was tested in ball-on-ring bending at a strain rate of $5 \times 10^{-5}$ per second instead of $5 \times 10^{-4}$ per second. One NKA alumina series was tested in four-point bending, one in three-point bending (short span) and one in ring-on-ring bending.

**Table 3.** Experimental conditions

| *Material* | *Test* | $n$ | $d\varepsilon/dt$ X10-5 | $v$ (*mm/min*) |
|---|---|---|---|---|
| Wesgo alumina | 3P20 | 39 | 4·6 | 2·23 |
| | 3P40 | 40 | 4·6 | 2·87 |
| | 4PB | 40 | 4·1 | 4·20 |
| | BOR1 | 40 | 0·5 | 0·31 |
| | BOR2 | 40 | 4·8 | 3·24 |
| | ROR | 36 | 5 | 14·00 |
| NKA alumina | 3P20 | 20 | 5 | 0·92 |
| | 4PB | 20 | 5 | 4·30 |
| | ROR | 20 | 5 | 14·40 |

$n$ = Number of specimens; $d\varepsilon/dt$ = strain rate; $v$ = cross-head speed of the test machine; 3P20/3P40 = three-point bend test at spans 20 and 40 mm; 4PB = four-point bend test (inner span 20 mm and outer span 40 mm); BOR = ball-on-ring test on ball-bearing support of 6 mm in radius; ROR = ring-on-ring test (inner ring 6 mm and outer ring 10 mm in radius).

## 2.3 Determination of the nominal fracture stress, $S_{nom}$

In the following $S_{nom}$ is defined as the nominal stress at fracture which corresponds to the extreme fibre fracture stress.

### *2.3.1 Three-point bending*

For three-point bending, the nominal fracture stress $S_{nom}$ was calculated using the simple beam theory but taking into account the Seewald–von Karman correction,[2]

$$S_{nom} = S_{max}\left(1 - 0{\cdot}266\frac{2h}{3s}\right) = \frac{3F_f s}{2wh^2}\left(1 - 0{\cdot}266\frac{2h}{3s}\right) \quad (1)$$

where $S_{max}$ is the maximum fibre stress according to the simple beam theory, $w$ and $h$ are the width and the height of the bar respectively, $s$ is the three-point bend span and $F_f$ is the fracture load.

### *2.3.2 Four-point bending*

For four-point bending the nominal fracture stress is equal to:

$$S_{nom} = S_{max} = \frac{3F_f(s_1 - s_2)}{2wh^2} \quad (2)$$

where $s_1$ and $s_2$ are the outer and the inner roller span.

*2.3.3 Ball-on-ring bending*

For ball-on-ring bending the nominal fracture stress is equal to:[3]

$$S_{nom} = \frac{3(1+\nu)F_f}{4\pi t^2}\left[1 + 2\ln\left(\frac{a}{b}\right) + \left(\frac{1-\nu}{1+\nu}\right)\left(\frac{a^2}{R^2}\right)\left(1 - \frac{b^2}{2a^2}\right)\right] \quad (3)$$

where $a$ is the support radius, $b$ the effective contact radius, $R$ the specimen radius, $t$ the specimen thickness and $\nu$ Poissons's ratio. According to de With and coworkers[2,4] it is sufficient to take the effective contact radius $b$ equal to one-third of the plate thickness, as it is assumed in the thin plate solution of the ball-on-ring test, which has been experimentally verified.[2]

*2.3.4 Ring-on-ring bending*

For ring-on-ring bending the nominal fracture stress is equal to:[3]

$$S_{nom} = \frac{3(1+\nu)F_f}{2\pi t^2}\left[\ln\left(\frac{a}{b}\right) + \left(\frac{1-\nu}{1+\nu}\right)\left(\frac{a}{R}\right)^2\left(\frac{1}{2} - \frac{1}{2}\left(\frac{b}{a}\right)^2\right)\right] \quad (4)$$

where $a$ is the support radius (outer ring), $b$ the loading ring radius (inner ring), $R$ the specimen radius, $t$ the specimen thickness and $\nu$ Poisson's ratio.

## 3 Statistical Procedure

### 3.1 Determination of Weibull parameters

The strength data were interpreted by means of the well-known two-parameter Weibull equation and the basic failure probability concept for surface flaws:

$$P_f = 1 - \exp\left[-\left(\frac{S_{nom}}{S_0}\right)^m\right] = 1 - \exp\left[-\left(\frac{1}{m}!\right)^m\left(\frac{S_{nom}}{\bar{S}_{nom}}\right)^m\right] \quad (5)$$

where $P_f$ is the failure probability, $S_{nom}$ is the nominal fracture stress obtained from the bend tests, $m$ is the Weibull modulus, $\bar{S}_{nom}$ the mean nominal fracture stress and $S_0$ is the characteristic strength.

A least-squares regression analysis with a weight factor[5] was used to estimate the population parameters $m$ and $S_0$. The strength data were ranked in ascending order and assigned a failure probability according to:

$$P_i = \frac{i - 0{\cdot}5}{n} \quad (6)$$

where $i$ is the order number and $n$ is the total number of specimens in the series. The applied weight factor is:

$$w_i = [(1 - P_i).\ln(1 - P_i)]^2 \quad (7)$$

Although this regression analysis is not standardized, it can be applied with confidence. Other fit procedures do not significantly affect the final result in this case. Moreover, Dortmans & de With[6] demonstrated that application of this probability index and weight factor together with a series size ($n$) greater than about 20 results in a Weibull modulus with a low bias for experiments with 1–2% accuracy. A series size of 40 was chosen for the Wesgo alumina while a series size of 20 was applied for the NKA material due to the limited availability. This study focuses on the extrapolation of mean fracture stresses from uniaxial to biaxial tests, which is not strongly dependent on the exact value of the Weibull modulus $m$.[7] Furthermore, it was observed that the scatter in $m$ for the NKA alumina is rather small (see Section 4) which justifies taking only 20 samples.

### 3.2 Predictions of the biaxial test results

The characteristic strengths of the alumina biaxial ball-on-ring and/or ring-on-ring tests were predicted using the Weibull parameters extracted from the uniaxial three-point and four-point bend tests. From the uniaxial tests, a mean Weibull modulus and characteristic strength of the unit surface for surface flaws was calculated. With these parameters the predictions were calculated applying two failure criteria: the mode I failure criterion (NSA), in which only normal stresses are considered, and the maximum noncoplanar strain energy release rate criterion (GMAX) for penny-shaped cracks according to Hellen & Blackburn.[8] The latter criterion incorporates shear stresses as well.

The calculations were performed with the finite element postprocessor FAILUR.[9] The finite element calculations were done with a finite element mesh such that

(1) the extreme fibre stress agrees with the analytical formulas given in Section 2.3, and
(2) the calculations were independent of the number of elements in the finite element mesh.

The mean nominal fracture stress, $\bar{S}_{nom}$, can be reformulated as:

$$\bar{S}_{nom} = S_u \left[ \frac{A_u}{A \,.\, \Sigma(A)} \right]^{1/m} = S_0 \left( \frac{1}{m}! \right)$$

$$= \int_0^{\infty} \frac{\delta P_f}{\delta S_{nom}} S_{nom} \, dS_{nom} \qquad (8)$$

in which $S_u$ is the unit strength for surface flaws, $A_u$ is the reference surface (unit surface) = 1, $A$ is the surface of the specimen and $\Sigma(A)$ is the surface stress integral:

$$\Sigma(A) = \frac{1}{A} \int_A \frac{1}{2\pi} \int_{C_u} \left( \frac{\sigma_{eq}}{S_{nom}} \right)^m dC_u \, dA \qquad (9)$$

where $C_u$ is the unit circle (radius 1) and $\sigma_{eq}$ the equivalent fracture stress. The equivalent fracture stress is taken as follows:

—for the mode I failure criterion (NSA)

$$\sigma_{eq} = \sigma_n \text{ if } \sigma_n \geq 0 \quad \text{and} \quad 0 \text{ if } \sigma_n < 0.$$

—for maximum noncoplanar energy release rate criterion (GMAX)

$$\sigma_{eq} = \sqrt[4]{\{\sigma_n^4 + 6\mu^2\sigma_n^2\tau^2 + \mu^4\tau^4\}} \text{ if } \sigma_n \geq 0$$

and $0$ if $\sigma_n < 0$

where

$$\mu = \left( \frac{2}{2 - \nu} \right)$$

for penny-shaped cracks, $\sigma_n$ and $\tau$ are the normal on and shear stress in the plane of a crack, and $\nu$ is Poisson's ratio.

## 4 Results and Discussion

The Weibull plots from the tests on the Wesgo and NKA alumina series are depicted in Figs 1 and 2 respectively. The Weibull moduli $m$ and associated standard deviation, the mean nominal strengths $\bar{S}_{nom}$ and the characteristic strengths $S_0$ are determined from these plots and are listed in Table 4, ranked in ascending order.

According to the Weibull theory, the tests should produce equal Weibull moduli if it is assumed that there is a single surface defect population that initiates failure. A bimodal defect population seems not very likely considering the Weibull plots. Unfortunately, this statement cannot be verified, since fractography on the tested specimens yielded no clear fracture origins. The weakest-link concept has also been applied using volume defects. This analysis showed no satisfying prediction at all.

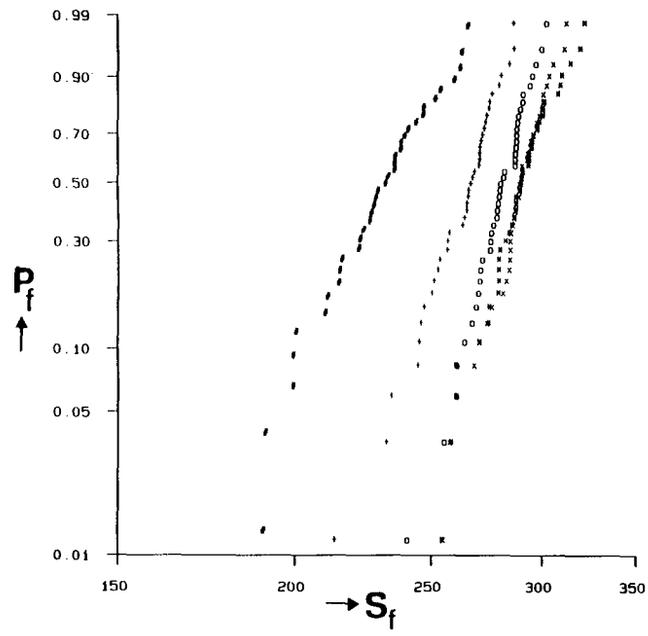


**Fig. 1.** Weibull plot of the bend tests on the Wesgo alumina. # = Ring-on-ring test; + = four-point bend test; 0 = three-point bend test at span length 40 mm; × = three-point bend test at span length 20 mm; * = ball-on-ring test.

When the characteristic strengths are ranked in ascending order, the test methods are ordered as follows: Ring-on-ring bending, four-point bending, three-point bending at span 40 mm, three-point bending at span 20 mm and ball-on-ring bending. This order is explained by the effective surface of the specimens, which is the largest in the ring-on-ring bend test and the smallest for the ball-on-ring bend test.

The standard deviation $\sigma$ in $m$ is approximately

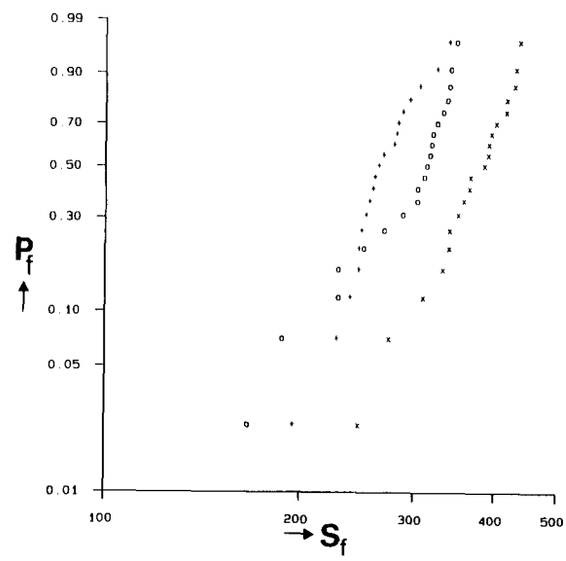


**Fig. 2.** Weibull plot of the bend tests on the NKA alumina. + = Ring-on-ring test; 0 = four-point bend test; × = three-point bend test at span length 20 mm.

**Table 4.** Weibull modulus $m$ (standard deviation between parentheses), mean nominal strength $\bar{S}_{nom}$ and characteristic strength $S_0$ from three-point bend tests at spans 20 and 40 mm (3P20 and 3P40), four-point bend tests (4PB), ball-on-ring tests (BOR) and ring-on-ring tests (ROR) on two aluminas

| | *Wesgo alumina* | | | *NKA alumina* | | |
|---|---|---|---|---|---|---|
| | $m$ | $\bar{S}_{nom}$ (*MPa*) | $S_0$ (*MPa*) | $m$ | $\bar{S}_{nom}$ (*MPa*) | $S_0$ (*MPa*) |
| ROR | 13·4 (2·2) | 229·8 | 238·9 | 9·0 (2·0) | 267·3 | 278·5 |
| 4PB | 21·6 (3·4) | 263·8 | 270·5 | 6·7 (1·5) | 298·8 | 320·2 |
| 3P40 | 27·1 (4·3) | 280·4 | 286·1 | | | |
| 3P20 | 27·3 (4·3) | 288·8 | 294·7 | 8·5 (1·9) | 371·3 | 393·1 |
| BOR1 | 21·8 (3·4) | 286·4 | 293·6 | | | |
| BOR2 | 21·6 (3·4) | 289·0 | 296·3 | | | |

equal to $m/N^{1/2}$ in which $N$ represents the number of measurements of a series.[6,7] For the NKA alumina, $m$ is equal for all test series within confidence bounds of $2\sigma$. The scatter in $m$ of the Wesgo alumina is somewhat greater. For this material the Weibull moduli agree within a confidence interval of $3\sigma$.

For the prediction of the biaxial data, the mean Weibull parameters $m$ (the Weibull modulus) and $S_u$ (the unit strength for surface flaws) were determined from the uniaxial data for the two models described in Section 3.2 (NSA and GMAX with a penny-shaped crack). The results are listed in Table 5. The deviation in $S_u$ and $\bar{S}_{nom}$ for the different uniaxial test series is about 1·5%, which is about the experimental accuracy. With these parameters the Wesgo alumina ball-on-ring and ring-on-ring experiments and the NKA alumina ring-on-ring experiments were predicted. The deviation of the predicted ball-on-ring and ring-on-ring mean nominal strengths from the measured values are listed in Table 6. The errors are calculated according to:

$$e = \frac{\bar{S}_{nom}^{pred} - \bar{S}_{nom}^{meas}}{\bar{S}_{nom}^{meas}} \times 100\% \qquad (10)$$

where the superscripts pred and meas denote the predicted and the measured values respectively.

It seems that for the Wesgo alumina the predictions are in good agreement with the NSA method (an error of −0·2% for the ring-on-ring and −0·5% for the ball-on-ring experiments), whereas the errors are large (error + 10% for the ring-on-ring and −30% for the ball-on-ring experiments) and significant with respect to the experimental error for the GMAX method. For the NKA alumina the opposite is the case. The GMAX method gives a good prediction for the ring-on-ring experiments (error −0·1%), whereas the NSA method gives a poor prediction (error −13%). This leads to the conclusion that the fracture mechanism of the NKA alumina is much more shear sensitive than that of the Wesgo alumina. An explanation for this feature is still missing, but can possibly be found in the following origins: (1) a different type of microstructure for the two aluminas (the Wesgo alumina having an unimodal and the NKA alumina a bimodal grain size distribution); (2) a difference in grain size, or (3) the presence of residual stresses due to the machining of the specimens.

Some other factors should be considered. Firstly, different green thicknesses for bars and disks may have affected the strength behaviour of the NKA alumina. During sintering different defect populations for bars and disks could be introduced. To the authors' opinion this seems not very likely, since $m$ is fairly equal for all test series. Moreover, the microstructures of both bars and disks are identical and isotropic.

Secondly, one might argue whether testing in dry

**Table 5.** Mean Weibull parameters $m$ and $S_u$ for the NSA and GMAX method, determined from the uniaxial test data (Table 3)

| *Material* | *NSA* | | *GMAX* | |
|---|---|---|---|---|
| | $m$ | $S_u$ (*MPa*) | $m$ | $S_u$ (*MPa*) |
| Wesgo alumina | 22·1 | 285·6 | 22·1 | 315·0 |
| NKA alumina | 8 | 423·4 | 8 | 489·1 |

NSA = Mode I failure; GMAX = maximum noncoplanar strain energy release rate for penny-shaped cracks.

**Table 6.** Deviation of the predicted ball-on-ring and ring-on-ring mean strengths from the measured values

| *Material* | *Test type* | *NSA error (%)* | *GMAX error (%)* |
|---|---|---|---|
| Wesgo alumina | BOR | −0·5 | −30 |
| | ROR | −0·2 | +10 |
| NKA alumina | ROR | −13 | −0·1 |

NSA = Mode I failure; GMAX = maximum noncoplanar strain energy release rate for penny-shaped cracks.

nitrogen prevents slow crack growth during the tests. The main goal was to perform each strength test under equal conditions, including relative humidity. It is expected that under the conditions used (dew point $-35°C$, strain rate $5 \times 10^{-4} s^{-1}$), slow crack growth plays no significant role. This seems to be confirmed by the equal strength values for the ball-on-ring tests performed on the Wesgo alumina at different strain rates.

Finally, the effect of *R*-curve behaviour should be mentioned. Although for different types of microstructure the *R*-curve is expected to be different, it is also expected that the influence of *R*-curve behaviour is small in view of the small original defect size. Moreover, for the Wesgo alumina no *R*-curve behaviour has been spotted by single-edge notched beam measurements with varying crack lengths (de Smet, B. J., 1991, pers. commun.). A more complete analysis will be done by applying additional failure criteria in subsequent work.[10] In the near future, tests on other materials will be done to investigate the effect of microstructure and residual stress on the various prediction methods.

## 5 Conclusions

Uniaxial and biaxial bend tests were performed on two aluminas with sufficiently high experimental accuracy. The Weibull characteristic strengths were ranked in the expected order and the Weibull moduli show good agreement. The predictions of the biaxial experiments from the uniaxial data series with the NSA and GMAX methods show that the best fitting failure criterion is different for both materials. The Wesgo alumina experiments are best predicted with the NSA method (non-shear sensitive, mode I failure) and the NKA alumina experiments with the GMAX method (shear sensitive, maximum non-coplanar strain energy release rate). In subsequent work, additional failure criteria for the present materials will be applied. Tests on other materials will be performed to see whether the best fitting failure criterion of a particular material can be related to its microstructural properties and/or residual stresses. For a successful approach, microstructures and residual stresses have to be quantified consistently.

## Acknowledgement

The work described in this paper has been partly sponsored by the Commission Innovative Research Program Technical Ceramics (IOP-TK) of the Ministry of Economic Affairs in The Netherlands (IOP-TK research grant 88.B040).

## References

1. Thiemeier, T., Brückner-Foit, A. & Kölner, H., Influence of the fracture criterion on the failure prediction of ceramics loaded in biaxial flexure. *J. Am. Ceram. Soc.*, **7**(4) (1991) 48–52.
2. Scholten, H., Dortmans, L., de With, G., de Smet, B. & Bach, P., Weakest-link failure prediction for ceramics II: Design and analysis of uniaxial and biaxial bend tests. Accepted *J. Eur. Ceram. Soc.*
3. Roark, R. J. & Young, W. C., *Formulas for stress and strain*, 5th edn. McGraw-Hill, Singapore, 1984.
4. de With, G. & Wagemans, H., Ball-on-ring test revisited. *J. Am. Ceram. Soc.*, **72** (1989) C1538–C1541.
5. Bergman, B., How to estimate Weibull parameters. *Brit. Ceram. Proceedings, Engineering with Ceramics*, **2** (1987) 39.
6. Dortmans, L. & de With, G., Noise sensitivity of fit procedures for Weibull parameter extraction. *J. Am. Ceram. Soc.*, **74**(9) (1991) 2293–4.
7. Quinn, G., Flexure strength of advanced structural ceramics: a round robin. *J. Am. Ceram. Soc.*, **73**(8) (1990) 2374–84.
8. Hellen, T. K. & Blackburn, W. S., The calculation of stress intensity factors for combined tensile and shear loading. *Int. J. Fracture*, **11**(4) (1975) 605–17.
9. Dortmans, L. & de With, G., Weakest-link failure predictions for ceramics using finite element post-processing. *J. Eur. Ceram. Soc.*, **6** (1990) 369–74.
10. Dortmans, L. & de With, G., Weakest-link failure prediction for ceramics IV: Application of mixed mode fracture criteria for multiaxial loading. *J. Eur. Ceram. Soc.*, **10** (1992) 109–14.